

A Microchambers Containing Contact Lens for the Noninvasive Detection of Tear Exosomes

Shaopei Li, Yangzhi Zhu,* Reihaneh Haghniaz, Satoru Kawakita, Shenghan Guan, Jianjun Chen, Zijie Li, Kalpana Mandal, Jamal Bahari, Shilp Shah, Juchen Guo, Heemin Kang, Wujin Sun, Han-Jun Kim, Vadim Jucaud, Mehmet R. Dokmeci, Pete Kollbaum, Chi Hwan Lee, and Ali Khademhosseini*

Exosomes, a form of small extracellular vesicles, play a crucial role in the metastasis of cancers and thus are investigated as potential biomarkers for cancer diagnosis. However, conventional detection methods like immune-based assay and microRNA analyses are expensive and require tedious pretreatments and lengthy analysis time. Since exosomes related to cancers are reported to exist in tears, a poly(2-hydroxyethyl methacrylate) contact lens embedded with antibody-conjugated signaling microchambers (ACSM-PCL) capable of detecting tear exosomes is reported. The ACSM-PCL exhibits high optical transparency and mechanical properties, along with extraordinary biocompatibility and good sensitivity to exosomes. A gold nanoparticle colorimetric assay is employed to visualize captured exosomes. The ACSM-PCL can detect exosomes in the pH range of 6.5–7.4 (similar to the human tear pH) and have a strong recovery yield in bovine serum albumin solutions. In particular, the ACSM-PCL can detect exosomes in various solutions, including regular buffer, cell culture media from various cell lines, and human tears. Finally, the ACSM-PCL can differentiate expression of exosome surface proteins hypothesized as cancer biomarkers. With these encouraging results, this ACSM-PCL is promised to be the next generation smart contact lens as an easy-to-use, rapid, noninvasive monitoring platform of cancer pre-screening and supportive diagnosis.


1. Introduction

Bodily fluid exosomes are becoming promising diagnostic targets for cancers such as breast cancer, hepatocellular carcinoma, and peripartum cardiomyopathy.^[1–8] These exosomes are produced during cellular externalization where their surface is enriched in proteins that are analogous to the secreting cells.^[9] Exosomes support various intercellular communications by carrying the necessary proteins, genetic materials, and lipid scaffolds to the recipient cells in a highly regulated manner.^[10,11] Evidence shows that host cells could relinquish their microRNA and messenger RNA into exosomes during the externalization process to pass on the genetic information to the recipient cells.^[12] Also, studies show that during the manifestation of cancers, organ injuries, and viral infections, specific proteins such as growth factors, survivins, and tetraspanins are present in

S. Li, Y. Zhu, R. Haghniaz, S. Kawakita, S. Guan, Z. Li, K. Mandal, J. Bahari, S. Shah, W. Sun, H.-J. Kim, V. Jucaud, M. R. Dokmeci, A. Khademhosseini
Terasaki Institute for Biomedical Innovation
Los Angeles, CA 90064, USA
E-mail: yzhu@terasaki.org; khademh@terasaki.org

J. Chen
Department of Chemical and Environmental Engineering
University of California
Riverside, CA 92521, USA

Z. Li, J. Guo
Mork Family Department of Chemical Engineering & Materials Science
Viterbi School of Engineering
University of Southern California
Los Angeles, CA 90007, USA

 The ORCID identification number(s) for the author(s) of this article can be found under <https://doi.org/10.1002/adfm.202206620>.

H. Kang
Department of Materials Science and Engineering
Korea University
Seoul 02841, Republic of Korea

W. Sun
Department of Biological System Engineering
Virginia Tech
Blacksburg, VA 24061, USA

P. Kollbaum
School of Optometry
Indiana University
Bloomington, IN 47408, USA

C. H. Lee
Weldon School of Biomedical Engineering
School of Mechanical Engineering
School of Materials Engineering
Purdue University
West Lafayette, IN 47907, USA

DOI: 10.1002/adfm.202206620

elevation on the surface and within the exosomes.^[13–16] Therefore, if exosomal proteins on the cell surface can be detected, then a novel generation of diagnostic approaches can be actualized. However, access to these potential biomarkers is limited mainly due to the isolating process of exosomes being tedious and time consuming.

Traditionally, the isolation of exosomes requires a pretreatment such as differential ultracentrifugation. Although effective, this approach causes isolated exosome samples to contain a high level of soluble protein and other cellular particle contaminants.^[17] Later approaches established a simpler isolation method by utilizing iodixanol solutions to achieve a density gradient, enabling clean and effective isolation of exosomes, but it still takes at least 10 h to complete this process.^[18]

There are several approaches to detect isolated exosomes. Most common one is the combination of flow cytometry and enzyme-linked assay (ELISA) kits that target the exosomal surface tetraspanins known as clusters of differentiation (CD): CD9, CD63, CD81, and CD82.^[19] These CDs rarely appear in other microvesicles, making them suitable candidates for quantifying the isolated exosomes. Emerging reports suggest that the utilization of unique CDs on exosomes to detect and quantify them has matured.^[20,21] Therefore, detecting exosomes other than particles per volume becomes feasible. However, the detection process also requires bulky and specialized equipment. Hence, if a device is capable of capturing and detecting exosomes with good portability, cost-effectiveness in a noninvasive manner, it will accelerate the exploration of exosome as a promising biomarker for cancers.

The source of exosome isolation is also of importance. Several bodily fluids hold high concentrations of exosomes, such as blood, urine, and saliva, however, tears are of great interest.^[22] Complex proximal fluids such as blood, urine, and saliva contain many interfering factors such as high levels of cellular debris, water or fat-soluble metabolite, and protease.^[23–28] In contrast, tears do not contain these elements; therefore, it is considered a “cleaner” fluid.^[29–31] This synergizes seamlessly with the contact lens (CL) biosensors.

CLs have been adopted as a platform with biosensing capabilities. Previous reports have demonstrated that CL biosensors can noninvasively monitor pH, ions, and biomolecules with high precision and good efficiency in tears.^[32–39] Previous CL biosensors were reported as a diagnostic tool for various ocular diseases.^[24,40,41] Among the diverse materials used to fabricate CLs, poly(2-hydroxyethyl methacrylate)(PHEMA) has been adopted as a CL material due to its superb mechanical property, excellent optical clarity, and biocompatibility.^[36,37,42]

Antibodies were utilized to detect exosomes due to their high specificity toward their cognate antigen.^[43–45] In addition, depending on the antigens, antibodies can be easily sourced through commercial channels. In the conventional approaches, antibody immobilization requires precious metallic or carbon nanomaterials to be integrated into the CL biosensor structure.^[35,46,47] Though the established covalent bond between the integrated metals and antibodies is robust, incorporating metallic or nanocarbon elements requires a clean-room facility, which increases their fabrication cost.^[48] Fortunately, chemical surface modification techniques for CLs have reached maturity, specifically, organosiloxane molecules are of interest. The Si–O

back bone of the organosiloxane molecule can form stable covalent bonding with any surface presented with OH moieties.^[49,50] Since the PHEMA surface is enriched in OH groups, this approach bypasses the need to incorporate metallic elements into the PHEMA CLs. In addition, integrating reactive amine groups on the organosiloxane molecule allows antibodies to attach onto PHEMA CLs with higher ease. With the incorporation of organosiloxane molecules for surface activation, a new series of cost-effective, scalable, and noninvasive CL biosensors can be constructed.

Herein, we demonstrate a PHEMA CL platform embedded with antibody-conjugated signaling microchambers (ACSM-PCL) for the specific and sensitive capture and detection of exosomes in tears. First, the PHEMA surface is activated by an organosiloxane molecule 3-triethoxysilyl propylsuccinic anhydride (TPSA). Next, anti-CD81 antibodies are immobilized onto the activated PHEMA surface for capturing exosomes. The unique expression of CD81 on the exosome surfaces will enable a specific capture of the exosomes.^[52,53] Gold nanoparticle (AuNP)-tagged anti-CD9 antibodies have been used to visualize the captured exosomes.^[54] To the best of our knowledge, no studies have attempted the capturing and quantifying of exosomes in tears using CLs. With further development, the reported ACSM-PCL platform can be easily repurposed for the clinical diagnosis of other diseases by using nanoparticle-conjugated antibodies specific for disease-related exosomes, thereby facilitating the establishment of a novel pre-screening tool for noninvasive clinical diagnosis.

2. Results and Discussion

2.1. Fabrication and Mechanism Revelation of ACSM-PCL

A homogeneous mixture of 2-hydroxyethyl methacrylate (HEMA, backbone monomer), ethyl glycol dimethacrylate (EDGMA, cross-linker), and 2-hydroxy-2-methylpropiophenone (Darocur 1173, photoinitiator) was injected into a lens-shaped mold and polymerized under ultraviolet (UV) irradiation to fabricate a CL. In contrast to conventional heat-induced polymerization, UV-induced polymerization yields CLs with higher optical clarity (Figure S1a,b, Supporting Information).

Next, microchambers were integrated onto the CL by direct laser cutting and engraving using a universal laser system (pattern is shown in Figure S1c, Supporting Information). Laser engraving preserves the microstructure without affecting the original structure and properties of the CL. Microchambers with a dimension of 50 μm in depth and 3 mm in diameter were placed at the boundary of CLs to provide a protective cavity where the antibodies are housed and cannot be rubbed off during contact with the cornea (Figure 1a). Since the human pupil has a diameter of 2–4 mm in ambient light and dilates in darker environments to 4–8 mm, the microchambers should be placed at the lens region around the iris only, so it would not obstruct vision. Finally, the microchambers were beveled to direct tear flowing into the sensor area.

As the last step to assemble ACSM-PCL, the surface of the microchambers within the PHEMA CL was modified. As shown in Figure 1b, the microchamber surfaces were activated

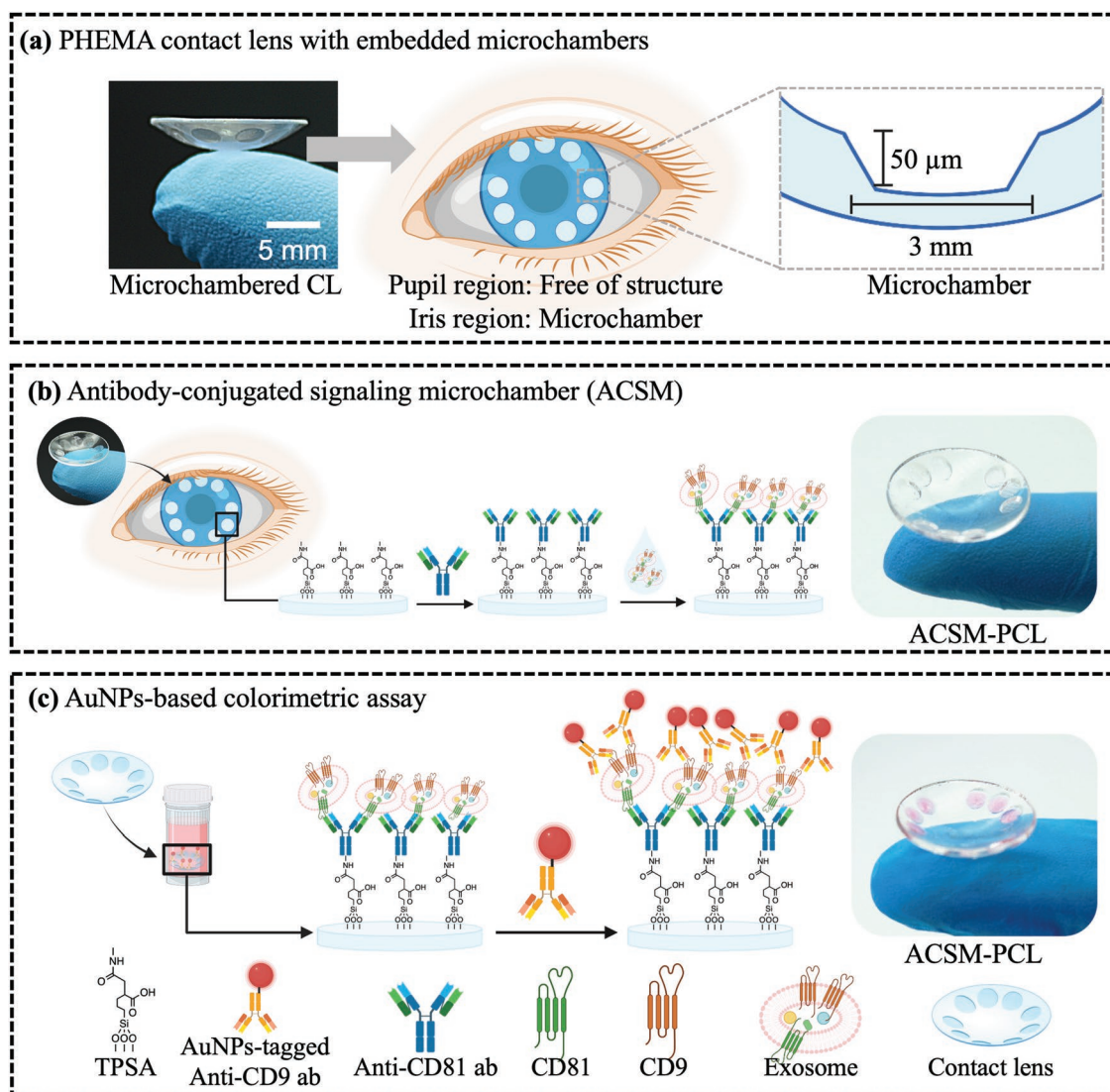


Figure 1. Schematic illustration of ACSM-PCL. a) PHEMA CL with embedded microchambers. The microchambers are placed at the boundary of the CL that is away from the pupil region. Therefore, it would not affect the eyesight of the wearers. b) Mechanism revelation of antibody-conjugating signaling microchambers within PHEMA CL. Anti-CD81 antibodies are covalently attached to the activated PHEMA CL surface and capture exosomes. c) Schematic illustration of the AuNP colorimetric assay. The captured tear exosomes are visualized using AuNP-tagged anti-CD9 antibodies.

using organosiloxane linkers. Organosiloxane molecules with a succinic moiety at the adjacent terminal were selected. This allowed the NH group on the exosome capture antibodies to react with the succinic moiety readily. In addition, the use of a succinic integrated organosiloxane linker eliminates the need to subject the CL surface to undergo the conventional amine coupling reaction for the antibody attachment, which reduces batch variation. Finally, once antibodies had functionalized the surface, ethanolamine was used to block the unreacted succinic surface. The final aspect of the ACSM-PCL platform is the detection of the captured exosomes. AuNPs are known to be utilized as a staining agent. Due to the surface plasmonic effect, AuNPs with a diameter of 50 nm have a unique rich red color with absorption at 550 nm.^[55] This unique character of AuNPs' red color has been adopted widely in both commercial products and literature to show the captured target.^[56–58] Also, AuNPs have previously been chemically stable and easily attached

with antibodies.^[59–61] Accordingly, we generated AuNPs tagged anti-CD9 antibodies to detect captured exosomes, as shown in Figure 1c. This ACSM-PCL provides a noninvasive, portable, and easily operable platform for a wide variety of clinical point-of-care diagnosis.

2.2. Surface Characterization of ACSM-PCL

The antibody immobilization on the PHEMA surface was first validated and optimized using phycoerythrin (PE) tagged anti-mouse IgG to stain the immobilized anti-CD81 antibodies, which accelerated the optimization of the immobilization process. An increasing concentration of anti-CD81 antibodies was added to the PHEMA surface after 3-triethoxysilyl propylsuccinic anhydride (TPSA) activation to optimize the antibody immobilization process. The result showed that 500 μg mL⁻¹ of anti-CD81

antibodies was the optimal concentration for immobilization (Figure S2, Supporting Information). Therefore, subsequent PHEMA has been modified accordingly.

Next, the surface modification process using X-ray photoelectric spectroscopy (XPS) to obtain the elemental information of the PHEMA surface is shown in Figure 2. Figure 2a shows the C 1s spectra of the PHEMA surface at each modification step. On the PHEMA surface (Figure 2a (i)), the C 1s XPS spectra revealed peaks at 289.48, 288.45, 286.48, and 284.68 eV corresponding to the carboxyl C=O, O–C=O, hydroxyl C–O, and the hydrocarbon C–C/C–H bonds, which is consistent with previous reports.^[62,63] With the addition of the TPSA linker to the surface (Figure 2a (ii)), an elevation of peak intensity at 284.68 eV was observed, correlating to the hydrocarbon moieties present on TPSA. This suggests that the modification has occurred. As anti-CD81 antibodies were added onto the surface (Figure 2a (iii)), the peaks at 289.48 eV increased, suggesting the increased presence of carboxyl groups found on the antibodies. These results demonstrated that the antibody attachment was successful. Finally, when the ethanolamine was added onto the surface (Figure 2a (iv)), the 288.45 eV peaks decreased, suggesting the ethanolamine had reacted with the remaining succinic moieties.

The incorporation of carboxyl containing elements from antibodies was also observed on the O1s spectra (Figure 2b). Where the 532.58 eV representative peak for the SiO₂ moiety shifted to lower than 531.68 eV suggesting organic C=O group is more present on the surface after anti-CD81 antibody attachment. In the silicon spectra, indications of successful surface modification were also observed. In Figure 2c, the PHEMA Si 2p spectra showed four peaks at 101.72, 102.08, 103.11, and 103.72 eV, corresponding to SiOC₃, SiO₂C₂, SiO₃C, and SiO₄ groups respectively.^[64] The presence of these groups was expected since polydimethylsiloxane (PDMS) molds were used to create the PHEMA CLs. Therefore, the observation of signals that correlate to polysiloxane structure is logical. After the PHEMA CL surface was incubated with the TPSA (Figure 2c (ii)), the peak at 101.72 eV increased. This can be correlated to the triethyl moieties on the TPSA, suggesting the successful surface activation of the PHEMA. The remaining Si 2p spectra (Figure 2c (iii-iv)) shows no further changes in peak position. This was attributed to the signal intensity variation to the additional layer of antibodies immobilized to the modified PHEMA surface. For the nitrogen spectra (Figure 2d (i-ii)), the PHEMA with and without using TPSA showed no observable nitrogen signal. After anti-CD81 antibodies were attached to the activated surface (Figure 2d (iii)), two peaks were found at 399.79 and 401.32 eV, corresponding to the amide and NH₂ groups present on the immobilized antibodies, respectively. Both peaks were still present after the surface was blocked using ethanolamine (Figure 2d (iv)), suggesting the blocking process did not alter the antibody layer. Based on the XPS spectra, it is highly likely that the immobilization process using TPSA as a surface modifier to attach antibodies, particularly the anti-human CD81 monoclonal antibody, was feasible and reliable. Additional survey scan on PHEMA CL surfaces that underwent the step-wise modification can be found in Figure S3 (Supporting Information) to show other elemental presence on the ACSM-PCL.

To further support the observation in XPS, energy-dispersive X-ray spectroscopy (EDX) analysis was performed

simultaneously to observe surface morphology. Carbon signal across all surfaces with a noticeable increase after each successive modification step (Figure S4a–d, Supporting Information) since more carbon-containing materials are deposited onto the surface. For PHEMA surfaces (Figure S4e, Supporting Information), a low level of silicon signal was found. After the surface had been modified with TPSA (Figure S4f, Supporting Information), an increase of silicon signal was noted. The presence of silicon signal was also observed for surface modification with anti-CD81 and ETA as shown in Figure S4g,h (Supporting Information). This suggests that the antibodies attachment and surface blocking did not alter the linker layer. Additionally, similar to the XPS result, a more indicative nitrogen signal was ascertained after anti-CD81 antibodies had been exposed to the microchamber surface as shown in Figure S4i–l (Supporting Information). This is parallel to the XPS results, suggesting successful functionalization of the PHEMA microchamber surfaces with antibodies. However, one primary concern when using organosiloxanes to modify surfaces is potential aggregations forming on the modified surface. From the EDX results, signal clusters were not observed, suggesting organosiloxane aggregation did not form. The SEM images with superimposed signal mapping (Si, O, N, and C) and the EDX spectra are summarized in Figure S5 (Supporting Information).

To demonstrate that the modification steps did not impair the surface, or the surface wettability, SEM and contact angle analysis were performed. As shown in Figure 2e, the SEM image for the surface at each step-wise modification showed no damage or altered surface morphology compared to the pristine PHEMA. This suggests that the modification did not damage the PHEMA surface. Then, through contact angle analysis shown in Figure 2f, the modified surface showed a contact angle of 41.31°–43.41°, similar to previous literature reports.^[51,65] Young's modulus was also obtained after modification steps, and optical transparency was measured. As shown in Figure S6a (Supporting Information), a negligible difference in the mechanical stiffness between the PHEMA surfaces after each modification step ($n = 3, p > 0.1$) was found. All PHEMA structures demonstrated an elastic modulus of 1.3–2.9 MPa, similar to previous report.^[66] This supports that the physical property was not altered during the modification process. Then the optical transparency was analyzed, as shown in Figure S6b (Supporting Information), a percent transmittance of light from 300 to 800 nm was measured. No significant decrease in the light transmittance was found until 347 nm, where only 50% of light transmittance was observed, suggesting that the lens structure can function over the visible light range. A swelling test was also done on the PHEMA surface. A 40% swelling of the mass was observed when examining the swelling ratio in both PBS buffer and water over a 24 h period at 37 °C (Figure S6c, Supporting Information). This confirms that the surface activation and antibody immobilization did not alter the physical structure of the PHEMA.

2.3. Biocompatibility of ACSM-PCL

PHEMA-containing CL has been approved by the U.S. Food and Drug Administration.^[48,67] During the design and construction of the ACSM-PCL, several features were integrated to

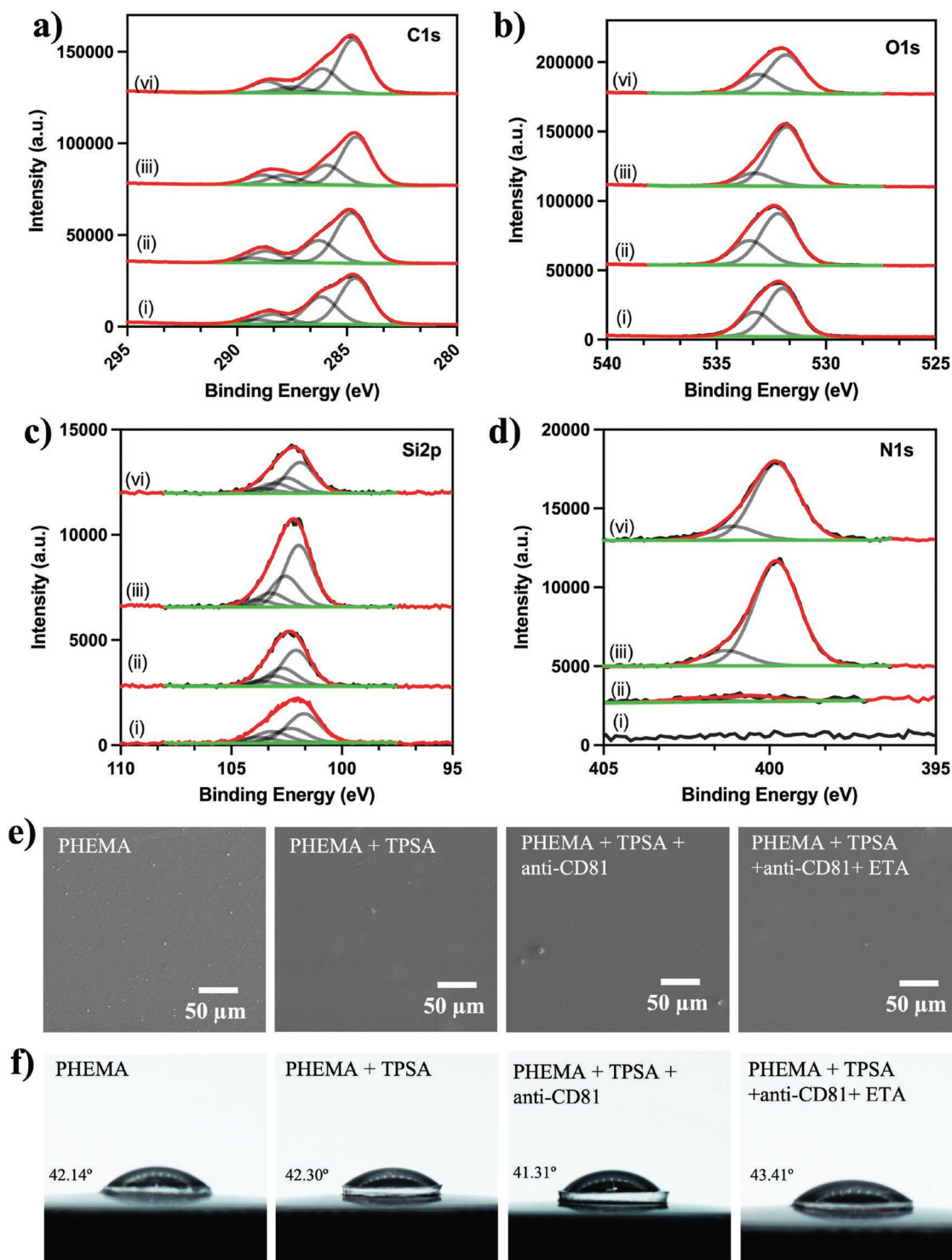


Figure 2. XPS and EDX analysis of ACSM-PCL. a) The C1s spectra, b) the O1s spectra, c) Si 2p spectra, and d) the N1s spectra are for (i) PHEMA microchamber surface, (ii) PHEMA with TPSA, (iii) PHEMA with TPSA and anti-CD81 antibodies and finally (iv) PHEMA surface with TPSA and anti-CD81 antibodies with ethanolamine (ETA) as a surface blocker. e) SEM image shows the surface in each modification step. f) The contact angle of the surface in stepwise modification.

ensure maximum wearing safety, for example, chambers with slanted walls to minimize sharp edges, and only the bottom of the chambers were chemically modified. However, to ensure the modification process and ACSM-PCL is safe for the eye, a

biocompatibility assay was performed using NIH/3T3 cell line. Representative images are shown in Figure S6a (Supporting Information). In Figure S6b (Supporting Information), day one after seeding, the percent viability of cells was at 96.2–99.9%.

On day 3, 97.7–99.3% of viability was observed, and finally, on day 7, the percent viability was observed at 95.0–98.3%. There was no significance in the cell viability between all the samples ($n = 3$, $p > 0.1$). These results suggest that the PHEMA modification did not cause cellular toxicity. This result is encouraging since CLs are usually worn for extended periods. If biocompatibility was an issue, it would affect the vision of the users and cause downstream health problems.

2.4. Analytical Performance of ACSM-PCL

AuNPs-tagged anti-CD9 antibodies were used as a visualization agent after the exosome was captured to increase the point-of-care potential and allow qualitative analysis through UV–vis spectroscopy. A series of control experiments were performed to determine the optimal anti-CD9 antibody concentration for detection. PE-conjugated anti-CD9 antibodies were used. After the ACSM-PCL was exposed to 0.1 mg mL⁻¹ of exosomes, Figure S8 (Supporting Information) shows that only positive control (10 μg of PE-tagged anti-CD9) and ACSM-PCL exhibited fluorescence. This suggests that the TPSA used to activate the PHEMA surface that was able to react with the NH₂ group on anti-CD81 antibodies. To further optimize the anti-CD9 antibodies concentration, increased PE-tagged anti-CD9 antibodies were used to stain the ACSM-PCL exposed to 0.1 mg mL⁻¹ of exosomes. In Figure S9 (Supporting Information), 10 μg mL⁻¹ yielded even and robust staining. AuNPs-tagged anti-CD9 antibodies were modified at this concentration in subsequent experiments. The UV–vis spectra of AuNPs after it was modified with anti-CD9 antibodies are shown in Figure S10 (Supporting Information). On the spectra, the AuNPs representative plasmonic absorption peak at $\lambda_{\text{max}} = 549$ nm undergoes a bathochromic shift to 557 nm. This observation aligns with previous reports where successful attachment of proteins can result in the change of the overall dimension of AuNPs, producing a shift on the visible spectrum.^[59,68,69] Therefore, the exosomes captured by anti-CD81 antibody immobilized on the ACSM-PCL microchamber can be quantified. **Figure 3a,b** shows the UV–vis spectra and the digital image of the PHEMA surface in different conditions. On the UV–vis spectra, the absence of exosomes was used as negative control (red curve), and no significant peaks were observed on the spectrum. In the positive control (0.025 mg mL⁻¹ of exosomes, blue curve), a peak at $\lambda_{\text{max}} = 557$ was observed. Finally, after the ACSM-PCL was incubated with 0.1 mg mL⁻¹ of exosomes and that a similar $\lambda_{\text{max}} = 557$ peak was observed, suggesting that exosomes were captured and detected by the ACSM-PCL.

We next examined the quantification ability of the ACSM-PCL. An increasing concentration of MCF-7 exosome standards (0.1–0.01 mg mL⁻¹) was incubated with the ACSM-PCL (Figure 3c). A Standard curved was obtained (Figure 3d), and there is direct linearity ($R^2 = 0.9936$, %CV = 5.72–2.00%) between exosome concentration and absorbance peak intensity. In addition, a calculated limit of detection was determined to be 2.14 μg mL⁻¹ using the formula $\text{LOD} = 3 \sigma m^{-1}$, where σ is the standard deviation of blank signal ($n = 5$), and m is the slope of the calibration curve.^[70,71] This result suggests that it is possible to employ the anti-CD81 modified

PHEMA surface as a sensor for exosome detection and quantifications.

To examine the performance of the ACSM-PCL, the detection of exosomes was evaluated in different pH environments (Figure 3e). Here, 0.01, 0.5, and 0.1 mg mL⁻¹ of exosomes were added to different phosphate buffered saline solutions (PBS) ranging from pH 6 to 8. The signal response in absorbance was obtained and plotted against the concentration. The slope of the signal response is extrapolated and plotted against the pH shown in Figure 3e. With increasing exosomes exposed to the sensor, pH 7.5, 7.0, and 6.5 showed a similar response. However, pH 8.0 and 6.0 demonstrated a smaller slope, suggesting a lower signal response in both pH environments. These results suggest that the optimal working pH environment for the sensor is between 6.5 and 7.5. Next, since human tears contain proteins such as serum albumin, the detection ability of exosomes by the ACSM-PCL in BSA-containing solution was also evaluated. The result shows the recovery percent by using the equations listed below:

$$\text{Percent recovery} = \frac{[\text{Analyte detected}]}{[\text{Analyte spiked in}]} * 100 \quad (1)$$

As shown in Figure 3f, a percent recovery of 112.1%, 109.8%, and 101.2% were found for solutions containing 5%, 3%, and 1% of BSA, respectively. Overall, the sensor can function in a controlled pH environment and BSA interference. The functional pH range of this ACSM-PCL falls well into the human tear pH range supporting the practicality of integrating the exosome sensor into the PHEMA CL.^[72]

Enzyme-linked immune assay (ELISA) has been the golden standard for exosome detections. To demonstrate that the reported ACSM-PCL system is comparable to a commercially available ELISA kit for exosome quantification, a comparison test was performed. Here, MCF 7 cancerous cell lines were selected due to their high rate of exosome secretion.^[73] First, the MCF 7 cell line was cultured to confluence, and the media were collected to quantify exosomes. As shown in Figure 3g, ACSM-PCL demonstrated similar performance to the ELISA kit ($n = 3$, $p < 0.1$). However, the result shows that ACSM-PCL demonstrated a higher coefficient of variation (CV) of 16% than the commercial ELISA kit at 8.9%. This result can be attributed to the variation introduced during the modification steps. For example, the reaction between the succinic group on TPSA and the anti-CD81 is randomized. Although this can be controlled to a certain extent by fine-tuning the reaction time and temperature, it can still cause variation between surface to surface. Hence, a larger CV was observed on the ACSM-PCL. However, CV may be drastically reduced as the fabrication process continues to improve by increasing the uniformity of the lens dimension and surface quality. In addition, automation of the incorporation of antibodies conjugated with succinic groups used to activate the ACSM-PCL surface will also drastically reduce CV. In addition, the commercial ELISA kit requires ≈4 h to complete the detection. The reported system only utilized almost half of the time the ELISA kit requires. Finally, it should be noted that after using AuNPs-tagged CD9 antibodies to visualize the captured exosomes, the optical clarity of the lens was not impacted (Figure 3h,i).

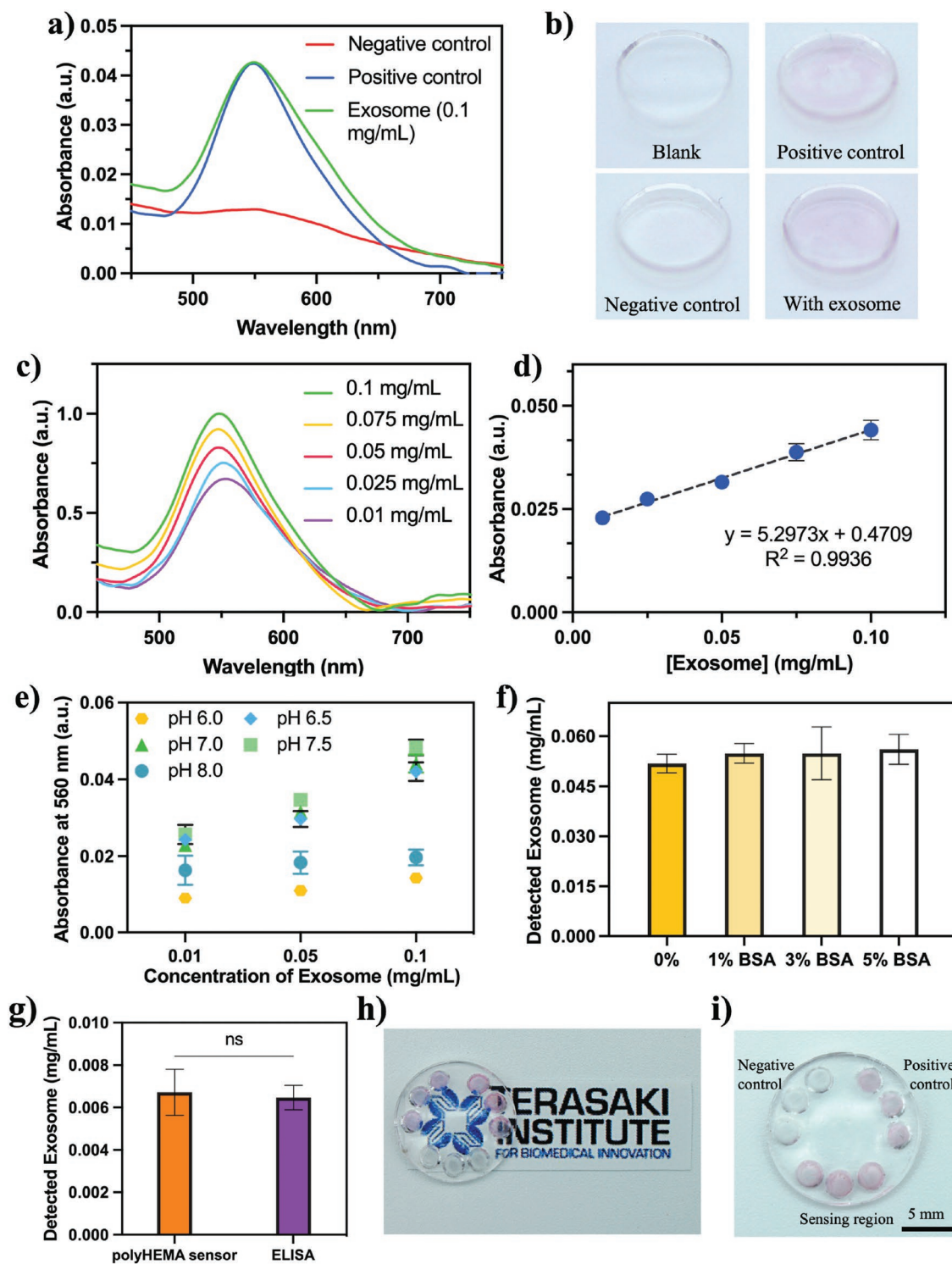


Figure 3. Analytical performance of ACSM-PCL. a) UV-vis spectrum of ACSM-PCL: no exosomes were present (red), exosome was immobilized (blue), and PHEMA sensor after exposed to 0.1 mg mL⁻¹ of exosomes (green). b) Digital image of the lens structure after AuNPs-tagged anti-CD9 visualization. c) UV-vis spectra of ACSM-PCL exposed to increasing concentration of MCF 7 exosome standards (0.1–0.01 mg mL⁻¹) and d) calibration plots of absorbance peak versus exosome concentration. e) ACSM-PCL response to increasing exosome concentration in different pH environments. f) Recovery yield of 0.0025 mg mL⁻¹ of exosome in solutions containing different percent (w/v) of BSA. g) Bar graph showing the performance comparison analysis between ACSM-PCL and (red column) commercially available ELISA plate on the exosome detection in MCF 7 human breast cancer cell line media. h) Shows a photographic image of the ACSM-PCL to detect artificial tear suspended exosomes, and i) shows the magnified view.

2.5. In Vitro Validation of ACSM-PCL

Exosome secretion rates are highly variable between cell types. Since the ACSM-PCL was designed to function as a robust exosome detection platform, it is critical to evaluate its capability to sense exosomes of different cellular origins. In addition, previous reports demonstrated that cancer could be detected through exosomes,^[9,74–76] and those cancer-derived exosomes have been found in tears.^[2,77–79] Here, ten different cell lines representing different physiological tissue and cancer types were selected and subjected to exosome detection. We selected cancerous cell line, U87 glioblastoma, MCF 7 tumorigenic breast cancer cells, MDAMB 231 metastatic breast cancer cells, HepG2 human liver cancer cells, ASPC-1 pancreatic tumor cells, and the following noncancerous cell line, MCF 10A Human mammary gland epithelial cell, HDF primary dermal fibroblast, HaCAT immortalized keratinocyte, Jurkat T-Cells, and human umbilical vein endothelial cells HUVECs. PBS was used as the blank control. If the sample media extract from the cultures was significantly different ($n = 3$, $p < 0.001$) in comparison to the negative control, it is determined as a positive reaction, reflecting the presence of exosomes in the sample. As shown in **Figure 4**, all the analyzed cell line supernatants demonstrated the presence of exosomes and confirmed exosome secretions. This was expected as all types of cells can release exosomes, but this result demonstrated that using anti-CD81 for capturing and anti-CD9 antibodies as the reporting element is an efficacious combination for the detection and quantification of exosomes. Indeed, different cell lines can express different levels of CD markers on the surface, resulting in variation during quantification. However, despite this deviation in CD markers expression, our reported system still holds its efficacy in detecting exosomes from different cell lines.

2.6. Validation of ACSM-PCL with Human Tears

Previously, breast cancer-secreted exosomes were detected in tears, by examining the breast cancer specific miR-21 and mrR-200c within exosomes.^[4,9,77] However, their process still requires differential centrifugation as a preisolation step of exosomes from tears prior to analysis of the internal contents, complicating the overall analysis procedure. Henceforth, ACSM-PCL was developed to demonstrate that both capture and detection of tear exosomes can be achieved. In this section, the tear of ten different volunteers was collected, then dropped into the sensing chamber and visualized using AuNPs-tagged-anti-CD9 antibodies. As shown in **Figure 5**, all the tear samples showed a detectable level of exosomes, as the sample signal is significantly different from the negative control ($p < 0.001$, additional results on statistical analysis are summarized in Table S1, Supporting Information). This result suggests that the proposed ACSM-PCL can detect exosomes in a small volume of real human tears. Nevertheless, these results are highly encouraging because AuNPs can be conjugated with other antibodies, we can easily substitute the anti-CD9 with other antibodies specific to disease-associated surface markers expressed on exosomes.

2.7. Differentiating Exosomes from Different Cell Lines

Previous literature has shown that human epidermal growth factor receptor 2 (HER2) and estrogen receptor (ER) are associated with cancer cell proliferation. Since exosomes can mirror their secreted cell, the captured exosomes from different cell lines can be characterized by changing the AuNPs-conjugated antibodies specific to these cancer biomarkers. In this section, three cell lines were chosen: MCF 10A (non-tumorigenic mammary gland epithelial cell line), MCF 7 (tumorigenic breast cancer cell line), and MDAMB 231 (Human Metastatic Breast Cancer Cell line). MCF 10A, as a non-tumorigenic cell line, is negative in HER2 and ER expression. In contrast, MCF 7 is known to express HER2 and ER.^[80,81] MDAMB231, though have been reported to be ER-negative, a low level of HER2 expression was found through immune histochemistry.^[82] Here, AuNPs-conjugated antibodies specific to HER2 and ER were made. As shown in **Figure 6**, the supernatant from the cell lines media MCF 10A, MCF 7, and MDAMB 231 was added onto the ACSM-PCL for exosome capture. Afterward, the surface was stained using AuNPs-conjugated HER2 antibodies, anti-ER, and anti-CD9 (a control to detect exosome presence). By extrapolating the $\lambda_{\text{max}} = 589$, $\lambda_{\text{max}} = 579$, and $\lambda_{\text{max}} = 560$ nm correlated to AuNPs-anti-HER2 Ab, AuNPs-anti-ER Ab, and AuNPs-anti-CD9 Ab, respectively. The result shows that all cell lines demonstrated positive CD9 expression, with MCF 7 positive for HER2 and ER expression; MDAMB 231 is positive for HER2. These results align with previous reports, where CD9 is a common surface protein for all exosomes, similar to the above sections. MCF10A was negative for both HER2 and ER expression. MCF 7 was positive in HER2 and ER expression. Interestingly, MDAMB 231 demonstrated a low expression of HER2. However, the significance between the negative control and the MDAMB 231 sample has a $p < 0.05$. Statistically, MDAMB 231 could also be considered negative in HER2 expression. Based on these preliminary results, the differentiation of surface protein expression on the isolated exosome between normal and cancerous cell lines is feasible using ACSM-PCL.

3. Conclusion

In conclusion, we developed an antibody-conjugated microchamber-based PHEMA CL platform to detect and capture intact exosomes in tears. The modification process of the PHEMA surface to become susceptible for anti-CD81 antibody functionalization has been demonstrated in this report. The resulting surface is stable and formed an even active layer of capturing antibodies. The fabricated ACSM-PCL is able to detect exosomes of different cellular origins effectively. An optimal pH environment of 6.5–7 for sensor function was determined, and it suggests that the biosensor performance is not affected by BSA. This indicates that the sensor performance is reliable in different environments. The ACSM-PCL can detect exosome secretions in nine different cell lines: U87, MCF 7, MDAMB 231, HepG2, ASPC-1, HDF, HaCAT T-Cells, and HUVECs. This shows that the anti-CD81 and anti-CD9 are proficient at exosome detection. The exosome detection performance of the

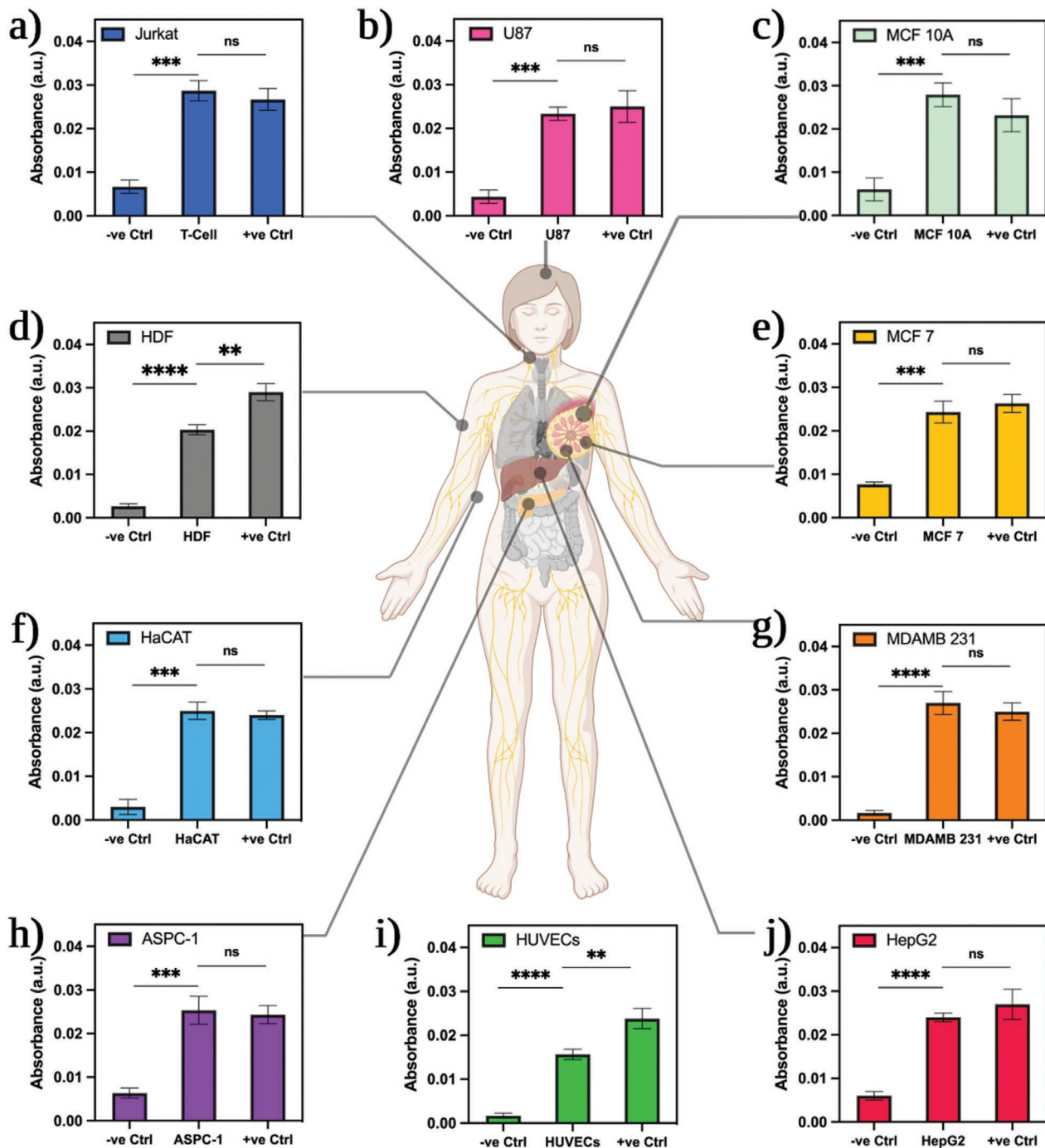


Figure 4. In vitro validation of ACSM-PCL with the cancer cell and noncancerous cell media. The exosome detection in different cell medias a) JURKAT T-Cells ($n = 3$, where *** represents $p = 0.0002$ for T-Cell versus negative control, *ns* where $p = 0.3679$ for T-Cell versus positive control). b) U87 Glioblastoma ($n = 3$, where *** represents $p = 0.0001$ for U87 versus negative control, *ns* where $p = 0.5$ for U87 versus positive control). c) MCF 10A Human mammary gland epithelial cell ($n = 3$, where *** represents $p = 0.0002$ for MCF 10A versus negative control, *ns* where $p = 0.1553$ for PBS versus positive control). d) HDF Primary Dermal Fibroblast ($n = 3$, where **** represents $p < 0.0001$ for HDF versus negative control, ** where $p = 0.0029$ for HDF versus positive control). e) MCF 7 Human tumorigenic breast cancer cells ($n = 3$, where *** represents $p = 0.0004$ for MCF 7 versus negative control, *ns* where $p = 0.3486$ for MCF 7 versus positive control). f) HaCAT Immortalized Keratinocyte cell line ($n = 3$, where *** represents $p = 0.0001$ for HaCAT versus negative control, *ns* where $p = 0.4818$ for HaCAT versus positive control). g) MDAMB 231 Human Metastatic Breast Cancer Cell line ($n = 3$, where **** represents $p < 0.0001$ for MDAMB 231 versus negative control, *ns* where $p = 0.3552$ for MDAMB 231 versus positive control). h) ASPC-1 pancreatic tumor cell line ($n = 3$, where ** represents $p = 0.0006$ for ASPC-1 versus negative control, *ns* where $p = 0.6745$ for ASPC-1 versus positive control). i) HUVECs ($n = 3$, where **** represents $p < 0.0001$ for HUVECs versus negative control, ** where $p = 0.0055$ for HUVECs versus positive control). j) HepG2 human liver cancer cell line ($n = 3$, where **** represents $p < 0.0001$ for HepG2 versus negative control, *ns* where $p = 0.2230$ for HepG2 versus positive control).

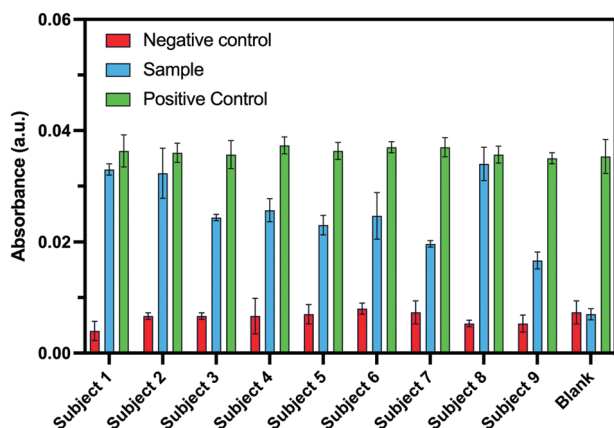


Figure 5. Validation of ACSM-PCL on exosome detection in human tear. Bar graph summarizing the exosome detection using the ACSM-PCL from nine human subjects. The tear samples were collected using microcapillary tubes and spun at 500 rpm for 1 min to obtain the tear sample. The error bar represents the standard deviation (SD) of $n = 3$, ns where $p > 0.5$, and **** where $p < 0.0001$. Additional details on the statistical analysis for significance can be found in Table S1 (Supporting Information).

ACSM-PCL in real human tears has also been analyzed, and the result shows that it is feasible to detect exosomes using the ACSM-PCL in human tear samples. Finally, utilizing anti-HER2 and anti-ER antibodies coated AuNPs, the ACSM-PCL demonstrated the exosome origin differentiation ability, further supporting its potential clinical applicability. It is important to note that the presented ACSM-PCL still requires signal amplification to increase the signal-to-noise ratio to be adopted into clinical settings. Secondary antibodies have been utilized to achieve this, in which the ACSM-PCL platform will continue to be optimized using this approach. Nevertheless, based on these results, the presented ACSM-PCL could capture, detect, and quantify exosomes in single CL structure without preisolations. This enables tear exosomes to be studied without introducing variations such as collection method or storage conditions. With these promising results, the detection of exosomes specific to cancers, viruses, and other diseases is underway in our labs. In future experiments, nanoparticle-conjugated antibodies will be used to detect disease-specific exosomes by this reported ACSM-PCL. Hence, with these encouraging results, the ACSM-PCL has the potential to become a powerful diagnostic tool for different diseases ranging from cancer to viral infections.

4. Experimental Section

XPS Analysis: X-ray photoelectric spectra were collected on a Thermo Scientific K-Alpha spectrometer with a monochromatic Al K α source (1486.6 eV). The accumulated angle was 90° with a 20 eV pass energy at the analyzer at a 10–8 mbar vacuum chamber.

Young's Modulus, Optical Transparency, and Contact Angle Measurement: The elastic modulus of PHEMA samples was measured using an Instron (5900 series) testing system. Each sample was fully saturated in DI water for over 12 h. The force and strain rate exerted on the samples were controlled using the Instron Bluehill 3 software. The calculation was performed using the governing equations below (or in the Supporting Information). All elastic modulus tests were operated in compressive

stress mode with 1 MPa min⁻¹ stress rate to ensure full elastic deformation. The governing equation for elastic modulus is:

$$E = \frac{\sigma}{\epsilon} = \frac{F/A}{\Delta L/L_0} \quad (2)$$

The stress, (σ), is calculated by force exerted on the sample, (F), divided by the cross-section area of samples (A), and strain, (ϵ), was characterized by the change of the grip displacement, ΔL , by the original thickness of the sample (L_0). The optical transparency was determined using Varioskan LUX multimode microplate reader (Thermo Fisher, MA USA) by measuring the transmittance from 300–800 nm. The contact angle was obtained using a Nikon D3400 DSLR camera fitted with a Tamron macro lens, and the obtained image was analyzed using Image J.

Scanning Electron Microscopy and Energy Dispersive X-Ray Analysis: Field emission scanning electron microscopy (FE-SEM, TESCAN, MIRA3, Brno, Czechia) equipped with EDX was used to obtain surface morphology and elemental information of the modified PHEMA structure.

Polymerization of 2-Hydroxyethyl Methacrylate: 3 mL of 2-hydroxyethyl methacrylate (HEMA, 98%, Sigma-Aldrich, MO USA) was combined with 25 μ L of ethyl glycol dimethacrylate (EGDMA, 98%, Sigma-Aldrich, MO USA) and 125 μ L 2-hydroxy-2-methylpropiophenone (Darocur 1173, 97%, Sigma-Aldrich, MO USA) to obtain a homogeneous mixture. The mixture was pipetted into molds made to the desired shape using polydimethylsiloxane (PDMS, SYLGARD 184 Silicone Elastomer Kit, Dow, MI USA) and cured in a UV-cross-linker chamber (Fisher Scientific, MA USA). The final PHEMA structure was cut to the desired shape using a laser cutter (Universal Laser System, AZ USA).

Surface Modification of ACSM-PCL for Exosome Detection: To modify the ACSM-PCL, 10% v/v of 3-triethoxysilyl propylsuccinic anhydride (TPSA, Gelest, PA USA) was mixed with DI water (18.4 Ω , Millipore Sigma, MA USA) and sonicated until the solution was clear and homogenous. The TPSA solution was drop cast onto the shaped PHEMA surface and incubated overnight at 4 °C. The PHEMA gels were thoroughly washed, and 30 μ g μ L⁻¹ of anti-HuCD81 antibodies (GeneTex, Low endotoxin, azide free, CA USA) was dropped-cast onto the activated surface and incubated at room temperature for 2 h. The modified surface was re-washed, and the unreacted succinic anhydride groups were blocked using 25 $\times 10^{-3}$ M ethanolamine. The anti-CD81 modified PHEMA was exposed to the exosome-containing sample and incubated at room temperature for 2 h (Lyophilized MCF-7 exosome standard (Abcam, Cambridge UK). Then the exposed surface was washed thoroughly using 1x PBS solution. Then, 5 μ L anti-CD9 antibody modified AuNPs was added onto the exosome exposed surface and incubated at room temperature for 30 min, then rinsed thoroughly before visualization using Varioskan LUX multimode microplate reader (Thermo Fisher, MA USA).

Modification of Anti-CD9 Antibodies Tagged Gold Nanoparticles (AuNPs): Using AuNPs with 60 nm in diameter (Sigma-Aldrich, MO USA), it was modified with anti-CD9 monoclonal antibodies (Santa Cruz Biotechnology, TX USA), Anti-ErBB2 (HER2) polyclonal antibodies (Thermo Scientific, MA USA) and anti-Estrogen Receptor Alpha monoclonal antibodies (GeneTex, Low endotoxin, azide free, CA USA) using methods described by Filbrun et al.^[59] Briefly, 200 μ L of the AuNP solutions were combined with 2 μ L of 0.5 $\times 10^{-3}$ M of 3,3'-dithiobis(sulfosuccinimidyl propionate) (DTSSP, Sigma-Aldrich, MO USA) solution. The mixture was incubated at room temperature under agitation for 1 h. The reacted mixture was centrifuged at 5000 g for 5 min, and the pellet was resuspended in 10 $\times 10^{-3}$ M PBS buffer solution. This step was repeated three times to wash away unreacted DTSSP, and then antibodies were added into the solution to achieve a final concentration of 5 μ g mL⁻¹ and incubated at room temperature for 1 h. The mixture was centrifuged at 5000 g for 5 min and washed using buffer solution. The modified AuNPs were resuspended in the desired pH 10 $\times 10^{-3}$ M PBS buffer solution and stored at 4 °C until used.

Cell Culture and Exosome Isolation: MCF 7 tumorigenic breast cancer cell line (HTB-22, ATCC, VA USA), MDAMB 231 (HTB-26, ATCC, VA USA), HaCAT Primary Human Epidermal Keratinocytes (PCS-200-011,

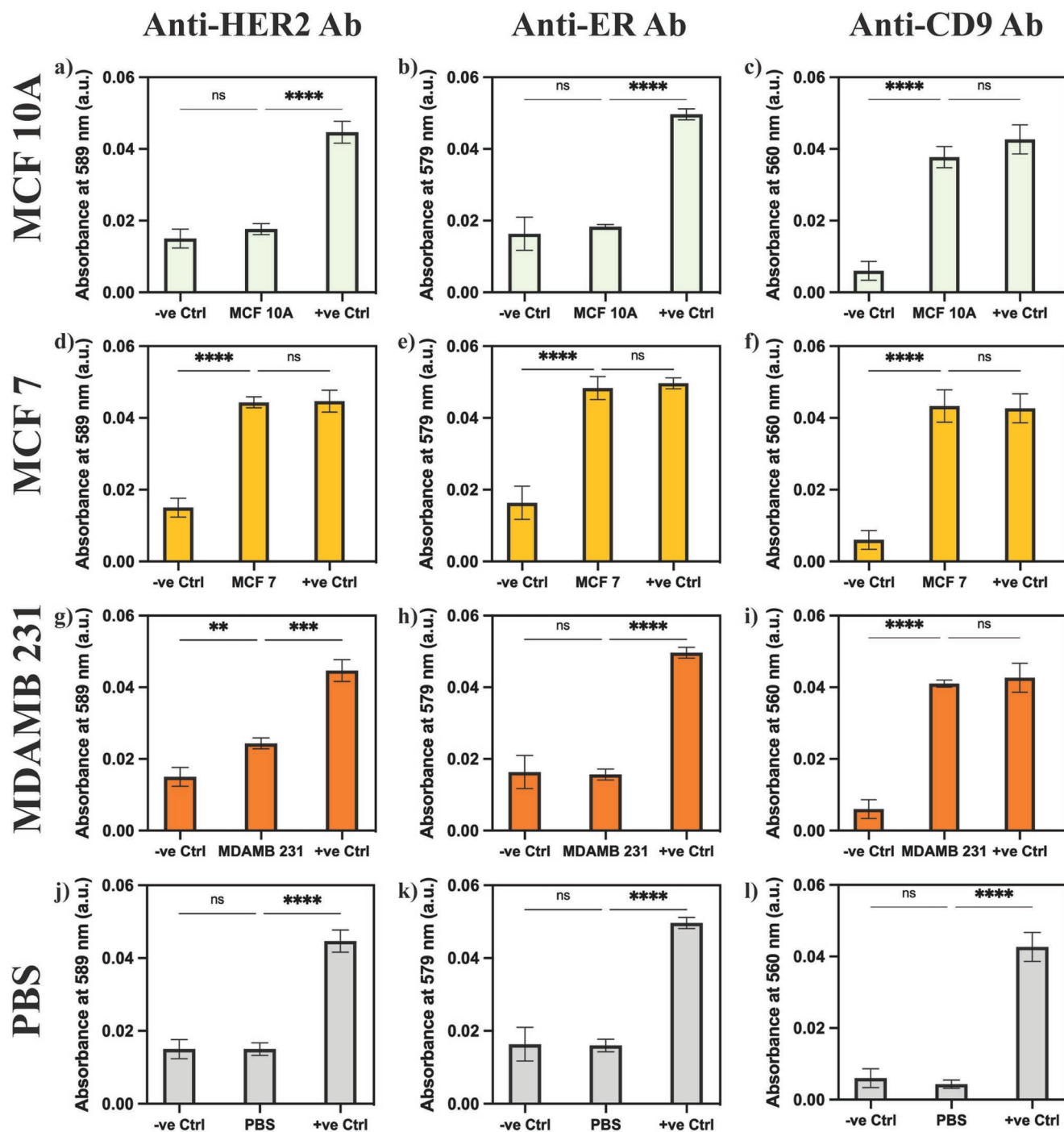


Figure 6. Differentiating exosome origin from between cell lines with ACSM-PCL. Bar graph representing the absorbance of different cell lines a–c) MCF 10A Human mammary gland epithelial cell, d–f) MCF 7 Human tumorigenic breast cancer cells, g–i) MDAMB 231 Human Metastatic Breast Cancer Cell line, j–l) 10×10^{-3} M PBS solution as blank. The error bar represents the standard deviation (SD) of $n = 3$, ns where $p > 0.5$, ** where $p < 0.005$, *** where $p = 0.0001$, and **** where $p < 0.0001$.

ATCC, VA USA), HDF Primary Human Dermal Fibroblast (PCS-201-012, ATCC, VA USA) and U87 Human Glioblastoma (HTB-14, ATCC, VA USA) were cultured in high Dulbecco's modified Eagle Medium (DMEM, Fisher Scientific, MA USA) with 10% Heat inactivated Fetal bovine serum (FBS, Life technologies, CA USA) and 1% penicillin-streptomycin (BioReagent, MS USA). Human umbilical cord vascular endothelium cells (HUVECs, CRL-1730, ATCC, VA USA) were cultured in Endothelial

cell growth medium (PromoCell, Germany). ASPC-1 Pancreatic tumor cells (CRL-1682, ATCC, VA USA) were cultured in RPMI-1640 media with L-glutamine (RPMI 1640, Cytiva, MA USA) with 10% Heat inactive FBS and 1% penicillin-streptomycin. HepG2 human liver carcinoma (HB-8065, ATCC, VA USA) were cultured in Minimum Essential Eagle Medium (MEM, Millipore Sigma, MO USA) with 10% Heat inactive FBS and 1% penicillin-streptomycin. Jurkat T Lymphoblast (T-cells)

(TIB-152, ATCC, VA USA) were cultured in RPMI-1640 media with L-glutamine (RPMI 1640, Cytiva, MA USA) with 10% FBS, 1% penicillin-streptomycin, and 1% HEPES Buffer (1 M, Fisher Scientific, NH USA). MCF 10A Human mammary gland epithelial cells (CRL-10317, ATCC, VA USA) were cultured in complete MCF 10A media (Elabscience, TX USA) that contained DMEM/F12 media base, 5% Horse Serum, 20 ng mL⁻¹ Epidermal Growth Factor, 100 ng mL⁻¹ Cholera Toxin, 0.5 ng mL⁻¹ Hydrocortisone, 10 µg mL⁻¹ insulin, 1% non-essential amino acid solution, 1% Penicillin-Streptomycin. All cells were grown at 37 °C in a humidified 5% CO₂ environment. The cells were grown to reach 99% confluency, and the media (12 mL) were collected. After media collections, the cells were detached by incubating with TrypLE (Thermo Fisher, MA USA) for 5 min and centrifuged at 120 g for 5 min. The isolated cells were counted using the Countess 3 Automated cell counter (Thermo Fisher, MA USA). Exosomes were isolated using Total Exosome Isolation Reagent (from cell culture media) (Invitrogen, MA USA) following the manufacture instructions. Briefly, the 1 mL of the culture media from the cells was combined with 500 µL of the isolation kit solution. After thoroughly mixed, the solution was incubated at 4 °C overnight and then centrifuged at 10 000× for 1 h at 4 °C. The supernatant was discarded, and the isolated exosomes were resuspended in 10 × 10⁻³ M PBS buffer, fresh cell culture media, and artificial tears, then stored at 4 °C until ready to be used.

Biocompatibility Assay: To assess the biocompatibility of the ACSM-PCL, NIH/3T3 cells (CRL-1658, ATCC, VA USA) were seeded into 48-well plates (Corning Inc. NY USA) with the ACSM-PCL, and LIVE/DEAD Viability/Cytotoxicity Kit (L3224, Invitrogen, MA USA) was used to stain live and dead cells at days 1, 3, and 7 following manufacture's protocol. Briefly, cells were washed with D-PBS, and 200 µL of a mixture of 4 × 10⁻⁶ M EthD-1 and ~2 × 10⁻⁶ M calcein-AM in D-PBS was added to each well. The cells were then incubated at 37 °C for 15 min, washed with D-PBS, and visualized under a fluorescence microscope. All samples were tested in triplicate. The acquired images were then processed using ImageJ to quantify % cell viability. Briefly, appropriate image adjustment and thresholding were made for each image, followed by a selection of the region of interest. Then, live and dead cells from each well were counted via the ImageJ's particle analysis function to calculate % cell viability.

Validation of Anti-CD81 Antibodies Immobilization Process: After the ACSM-PCL was activated using TPSA, an increasing concentration of anti-CD81 antibodies (500–100 µg) was added to the activated surface. Then, 10, 5, and 2.5 mg mL⁻¹ of R-Phycoerythrin-conjugated Fragment Goat Anti-Mouse IgG (Jackson Immuno Research Lab, PA USA) were added to the surface and incubated at room temperature for 30 min. An optimal concentration of 5 mg mL⁻¹ was determined and used in the staining process and subsequent experiments. The stained ACSM-PCL was visualized on a customized microscope.

Human Tear Collection: All tear samples were collected from nine subjects. The tear was collected using homemade microcapillary tubes by holding the microcapillary tubes gently against the corner of the eyes to allow capillary action to direct the flow of tears into the tube. Then, the tubes were gently centrifuged at 100 rpm into 1.5 mL Eppendorf tubes (Millipore Sigma, MA USA). The tear sample was introduced into the microchamber for further exosome detection. Real-sample evaluation was performed on adult individuals with the protocol approved by the institutional review board at the Indiana University (IRB#2 004 308 902).

Statistical Analysis: UV-vis results were background subtracted by using 0.01 M PBS as the standard blank solution, measured the absorbance between 250 and 900 nm. All experiments were performed in triplicates ($n = 3$) to calculate the mean, with error bars representing the standard deviation (\pm SD). Significance analysis by two-way analysis of variance (2-way ANOVA) was performed using Graph Pad Software (CA, USA). Statistics of group ($n = 3$) were considered significant when $p < 0.05$ or less, with $\alpha = 0.05$.

Supporting Information

Supporting Information is available from the Wiley Online Library or from the author.

Acknowledgements

The authors acknowledge the colleagues from the Terasaki Institute for Biomedical Innovation, the University of California, San Diego, and the University of California, Riverside, for helpful discussions.

Conflict of Interest

The authors declare no conflict of interest.

Data Availability Statement

The data that support the findings of this study are available from the corresponding author upon reasonable request.

Keywords

biomarkers, biosensors, cancer diagnosis, contact lenses, exosomes, wearables

Received: June 10, 2022

Revised: July 13, 2022

Published online:

- [1] W. Sun, J.-d. Luo, H. Jiang, D. D. Duan, *Acta Pharmacol. Sin.* **2018**, *39*, 534.
- [2] T. Takeuchi, K. Mori, H. Sunayama, E. Takano, Y. Kitayama, T. Shimizu, Y. Hirose, S. Inubushi, R. Sasaki, H. Tanino, *J. Am. Chem. Soc.* **2020**, *142*, 6617.
- [3] R. Kalluri, V. S. LeBleu, *Science* **2020**, *367*, eaau6977.
- [4] Y. Jia, Y. Chen, Q. Wang, U. Jayasinghe, X. Luo, Q. Wei, J. Wang, H. Xiong, C. Chen, B. Xu, W. Hu, L. Wang, W. Zhao, J. Zhou, *Oncotarget* **2017**, *8*, 41717.
- [5] J. S. Schorey, S. Bhatnagar, *Traffic* **2008**, *9*, 871.
- [6] E. G. Trams, C. J. Lauter, N. Salem, U. Heine, *Biochim. Biophys. Acta (BBA) – Biomembr.* **1981**, *645*, 63.
- [7] J. Halkein, S. P. Tabruyn, M. Ricke-Hoch, A. Haghikia, N.-Q.-N. Nguyen, M. Scherr, K. Castermans, L. Malvaux, V. Lambert, M. Thiry, K. Sliwa, A. Noel, J. A. Martial, D. Hilfiker-Kleiner, I. Struman, *J. Clin. Invest.* **2013**, *123*, 2143.
- [8] T. Kogure, W.-L. Lin, I. K. Yan, C. Braconi, T. Patel, *Hepatology* **2011**, *54*, 1237.
- [9] P. Jenjaroenpun, Y. Kremenska, V. M. Nair, M. Kremensky, B. Joseph, I. V. Kurochkin, *PeerJ* **2013**, *1*, e201.
- [10] C. Théry, M. Boussac, P. Véron, P. Ricciardi-Castagnoli, G. Raposo, J. Garin, S. Amigorena, *J. Immunol.* **2001**, *166*, 7309.
- [11] C. Théry, L. Zitvogel, S. Amigorena, *Nat. Rev. Immunol.* **2002**, *2*, 569.
- [12] C. Aslan, S. H. Kiaie, N. M. Zolbanin, P. Lotfinejad, R. Ramezani, F. Kashanchi, R. Jafari, *BMC Biotechnol.* **2021**, *21*, 20.
- [13] H. Peinado, M. Alečković, S. Lavotshkin, I. Matei, B. Costa-Silva, G. Moreno-Bueno, M. Hergueta-Redondo, C. Williams, G. García-Santos, C. M. Ghajar, A. Nitoro-Hoshino, C. Hoffman, K. Badal, B. A. Garcia, M. K. Callahan, J. Yuan, V. R. Martins, J. Skog, R. N. Kaplan, M. S. Brady, J. D. Wolchok, P. B. Chapman, Y. Kang, J. Bromberg, D. Lyden, *Nat. Med.* **2012**, *18*, 883.
- [14] J. Skog, T. Würdinger, S. van Rijn, D. H. Meijer, L. Gainche, W. T. Curry, B. S. Carter, A. M. Krichevsky, X. O. Breakefield, *Nat. Cell Biol.* **2008**, *10*, 1470.

- [15] H. Zhou, T. Pisitkun, A. Aponte, P. S. Yuen, J. D. Hoffert, H. Yasuda, X. Hu, L. Chawla, R. F. Shen, M. A. Knepper, R. A. Star, *Kidney Int.* **2006**, *70*, 1847.
- [16] S. Sadeghipour, R. A. Mathias, *Semi.Cell Dev. Biol.* **2017**, *67*, 91.
- [17] C. Théry, S. Amigorena, G. Raposo, A. Clayton, *Curr. Protoc. Cell Biol.* **2006**, *30*, 3.22.1.
- [18] P. Li, M. Kaslan, S. H. Lee, J. Yao, Z. Gao, *Theranostics* **2017**, *7*, 789.
- [19] Z. Andreu, M. Yáñez-Mó, *Front. Immun.* **2014**, *5*.
- [20] B. S. Chia, Y. P. Low, Q. Wang, P. Li, Z. Gao, *TrAC Trends Anal. Chem.* **2017**, *86*, 93.
- [21] M. Macías, V. Rebmann, B. Mateos, N. Varo, J. L. Perez-Gracia, E. Alegre, Á. González, *Clin. Chem. Lab. Med.* **2019**, *57*, 1539.
- [22] N. P. Hessvik, A. Llorente, *Cell. Mol. Life Sci.* **2018**, *75*, 193.
- [23] M. E. Stern, J. Gao, K. F. Siemasko, R. W. Beuerman, S. C. Pflugfelder, *Exp. Eye Res.* **2004**, *78*, 409.
- [24] Z. Ballard, S. Bazargan, D. Jung, S. Sathianathan, A. Clemens, D. Shir, S. Al-Hashimi, A. Ozcan, *Lab Chip* **2020**, *20*, 1493.
- [25] S. R. Corrie, J. W. Coffey, J. Islam, K. A. Markey, M. A. Kendall, *Analyst* **2015**, *140*, 4350.
- [26] A. Singh, A. Sharma, A. Ahmed, A. K. Sundramoorthy, H. Furukawa, S. Arya, A. Khosla, *Biosensors* **2021**, *11*, 336.
- [27] A. Sharma, A. Agrawal, K. K. Awasthi, K. Awasthi, A. Awasthi, *Mater. Lett.: X* **2021**, *10*, 100077.
- [28] J. Kim, G. Valdes-Ramirez, A. J. Bandodkar, W. Jia, A. G. Martinez, J. Ramirez, P. Mercier, J. Wang, *Analyst* **2014**, *139*, 1632.
- [29] M. L. Y. Sin, K. E. Mach, P. K. Wong, J. C. Liao, *Expert Rev. Mol. Diagn.* **2014**, *14*, 225.
- [30] M. Ouyang, D. Tu, L. Tong, M. Sarwar, A. Bhimaraj, C. Li, G. L. Coté, D. Di Carlo, *Biosens. Bioelectron.* **2021**, *171*, 112621.
- [31] H. Ehtesabi, *Mater. Today Chem.* **2020**, *17*, 100342.
- [32] A. K. Yetisen, N. Jiang, C. M. Castaneda Gonzalez, Z. I. Erenoglu, J. Dong, X. Dong, S. Stosser, M. Brischwein, H. Butt, M. F. Cordeiro, M. Jakobi, O. Hayden, A. W. Koch, *Adv. Mater.* **2020**, *32*, 1906762.
- [33] R. Badugu, B. H. Jeng, E. A. Reece, J. R. Lakowicz, *Anal. Biochem.* **2018**, *542*, 84.
- [34] J. Park, J. Kim, S.-Y. Kim, W. H. Cheong, J. Jang, Y.-G. Park, K. Na, Y.-T. Kim, J. H. Heo, C. Y. Lee, J. H. Lee, F. Bien, J.-U. Park, *Sci. Adv.* **2018**, *4*, eaap9841.
- [35] D. H. Keum, S. K. Kim, J. Koo, G. H. Lee, C. Jeon, J. W. Mok, B. H. Mun, K. J. Lee, E. Kamrani, C. K. Joo, S. Shin, J. Y. Sim, D. Myung, S. H. Yun, Z. Bao, S. K. Hahn, *Sci. Adv.* **2020**, *6*, eaba3252.
- [36] Y. Zhu, S. Li, J. Li, N. Falcone, Q. Cui, S. Shah, M. C. Hartel, N. Yu, P. Young, N. R. de Barros, *Adv. Mater.* **2018**, *30*, 2108389.
- [37] Y. Zhu, R. Haghniaz, M. C. Hartel, L. Mou, X. Tian, P. R. Garrido, Z. Wu, T. Hao, S. Guan, S. Ahadian, H.-J. Kim, V. Jucaud, M. R. Dokmeci, A. Khademhosseini, *ACS Biomater. Sci. Eng.* **2021**.
- [38] K. Kim, H. J. Kim, H. Zhang, W. Park, D. Meyer, M. K. Kim, B. Kim, H. Park, B. Xu, P. Kollbaum, B. W. Boudouris, C. H. Lee, *Nat. Commun.* **2021**, *12*, 1544.
- [39] Y. Zhu, M. C. Hartel, N. Yu, P. R. Garrido, S. Kim, J. Lee, P. Bandaru, S. Guan, H. Lin, S. Emaminejad, N. R. de Barros, S. Ahadian, H.-J. Kim, W. Sun, V. Jucaud, M. R. Dokmeci, P. S. Weiss, R. Yan, A. Khademhosseini, *Small Methods* **2022**, *6*, 2100900.
- [40] C. Song, G. Ben-Shlomo, L. Que, *J. Microelectromech. Syst.* **2019**, *28*, 810.
- [41] M. Ku, J. Kim, J.-E. Won, W. Kang, Y.-G. Park, J. Park, J.-H. Lee, J. Cheon, H. H. Lee, J.-U. Park, *Sci. Adv.* **2020**, *6*, eabb2891.
- [42] X. Ma, S. Ahadian, S. Liu, J. Zhang, S. Liu, T. Cao, W. Lin, D. Wu, N. R. de Barros, M. R. Zare, S. E. Diltemiz, V. Jucaud, Y. Zhu, S. Zhang, E. Banton, Y. Gu, K. Nan, S. Xu, M. R. Dokmeci, A. Khademhosseini, *Adv. Intell. Syst.* **2021**, *3*, 2000263.
- [43] J. Kim, A. S. Campbell, B. E.-F. de Ávila, J. Wang, *Nat. Biotechnol.* **2019**, *37*, 389.
- [44] E. Cesewski, B. N. Johnson, *Biosens. Bioelectron.* **2020**, *159*, 112214.
- [45] X. Tao, X. Wang, B. Liu, J. Liu, *Biosens. Bioelectron.* **2020**, *168*, 112537.
- [46] J. Jang, J. Kim, H. Shin, Y.-G. Park, B. J. Joo, H. Seo, J.-e. Won, D. W. Kim, C. Y. Lee, H. K. Kim, J.-U. Park, *Sci. Adv.* **2021**, *7*, eabf7194.
- [47] H. Zhang, R. He, Y. Niu, F. Han, J. Li, X. Zhang, F. Xu, *Biosens. Bioelectron.* **2022**, *197*, 113777.
- [48] Y. Zhu, S. Li, J. Li, N. Falcone, Q. Cui, S. Shah, M. C. Hartel, N. Yu, P. Young, N. R. de Barros, Z. Wu, R. Haghniaz, M. Ermis, C. Wang, H. Kang, J. Lee, S. Karamikamkar, S. Ahadian, V. Jucaud, M. R. Dokmeci, H.-J. Kim, A. Khademhosseini, *Adv. Mater.* **2022**, *34*, 2108389.
- [49] A. Gang, G. Gabernet, L. D. Renner, L. Baraban, G. Cuniberti, *RSC Adv.* **2015**, *5*, 35631.
- [50] X. Huang, A. Schmucker, J. Dyke, S. M. Hall, J. Retrum, B. Stein, N. Remmes, D. V. Baxter, B. Dragnea, L. M. Bronstein, *J. Mater. Chem.* **2009**, *19*, 4231.
- [51] Y. Chen, S. Zhang, Q. Cui, J. Ni, X. Wang, X. Cheng, H. Alem, P. Tebon, C. Xu, C. Guo, R. Nasiri, R. Moreddu, A. K. Yetisen, S. Ahadian, N. Ashammakhi, S. Emaminejad, V. Jucaud, M. R. Dokmeci, A. Khademhosseini, *Lab Chip* **2020**, *20*, 4205.
- [52] M. Zöller, *Nat. Rev. Cancer* **2009**, *9*, 40.
- [53] G. Raposo, W. Stoorvogel, *J. Cell Biol.* **2013**, *200*, 373.
- [54] V. Parthasarathy, F. Martin, A. Higginbottom, H. Murray, G. W. Moseley, R. C. Read, G. Mal, R. Hulme, P. N. Monk, L. J. Partridge, *Immunology* **2009**, *127*, 237.
- [55] L. A. Dykman, N. G. Khlebtsov, *Acta Naturae* **2011**, *3*, 34.
- [56] W. C. Mak, V. Beni, A. P. F. Turner, *TrAC Trends Anal. Chem.* **2016**, *79*, 297.
- [57] L. Rivas, A. d. I. Escosura-Muñiz, J. Pons, A. Merkoçi, in *Comprehensive Analytical Chemistry*, Vol. 66, (Eds: M. Valcárcel, Á. I. López-Lorente), Elsevier, Amsterdam **2014**, p. 569.
- [58] P. Baptista, E. Pereira, P. Eaton, G. Doria, A. Miranda, I. Gomes, P. Quaresma, R. Franco, *Anal. Bioanal. Chem.* **2008**, *391*, 943.
- [59] S. L. Filbrun, A. B. Filbrun, F. L. Lovato, S. H. Oh, E. A. Driskell, J. D. Driskell, *Analyst* **2017**, *142*, 4456.
- [60] M. H. Jazayeri, H. Amani, A. A. Pourfatollah, H. Pazoki-Toroudi, B. Sedighmoghaddam, *Sens. Bio-Sens. Res.* **2016**, *9*, 17.
- [61] S. B. Geng, J. Wu, M. E. Alam, J. S. Schultz, C. D. Dickinson, C. R. Seminer, P. M. Tessier, *Bioconjugate Chem.* **2016**, *27*, 2287.
- [62] L. Wang, C. Lu, H. Liu, S. Lin, K. Nan, H. Chen, L. Li, *RSC Adv.* **2016**, *6*, 1194.
- [63] S. L. McArthur, K. M. McLean, H. A. W. S. t. John, H. J. Griesser, *Biomaterials* **2001**, *22*, 3295.
- [64] S. Roualdes, R. Berjoan, J. Durand, *Sep. Purif. Technol.* **2001**, *25*, 391.
- [65] J. D. Andrade, R. N. King, D. E. Gregonis, D. L. Coleman, *J. Polym. Sci.: Polym. Symp.* **1979**, *66*, 313.
- [66] G. Li, I. Dobryden, E. J. Salazar-Sandoval, M. Johansson, P. M. Claesson, *Soft Matter* **2019**, *15*, 7704.
- [67] M. Zare, A. Bigham, M. Zare, H. Luo, E. Rezvani Ghomi, S. Ramakrishna, *Int. J. Mol. Sci.* **2021**, *22*, 6376.
- [68] L. Anfossi, C. Baggiani, C. Giovannoli, G. Giraudi, *Anal. Bioanal. Chem.* **2009**, *394*, 507.
- [69] X. Cui, M. Liu, B. Li, *Analyst* **2012**, *137*, 3293.
- [70] Á. Lavín, J. D. Vicente, M. Holgado, M. F. Laguna, R. Casquel, B. Santamaría, M. V. Maigler, A. L. Hernández, Y. Ramírez, *Sensors* **2018**, *18*, 2038.
- [71] D. A. Armbruster, M. D. Tillman, L. M. Hubbs, *Clin. Chem.* **1994**, *40*, 1233.
- [72] M. B. Abelson, I. J. Udell, J. H. Weston, *Arch. Ophthalmol.* **1981**, *99*, 301.
- [73] J. Dai, Y. Su, S. Zhong, L. Cong, B. Liu, J. Yang, Y. Tao, Z. He, C. Chen, Y. Jiang, *Signal Transduct. Target Ther.* **2020**, *5*, 145.
- [74] H. Wang, Z. Lu, X. Zhao, *J. Hematol. Oncol.* **2019**, *12*, 133.

- [75] L. Rios-Colon, E. Arthur, S. Niture, Q. Qi, J. T. Moore, D. Kumar, *Cells* **2020**, *9*, 1988.
- [76] B. Costa-Silva, N. M. Aiello, A. J. Ocean, S. Singh, H. Zhang, B. K. Thakur, A. Becker, A. Hoshino, M. T. Mark, H. Molina, *Nat. Cell Biol.* **2015**, *17*, 816.
- [77] S. Inubushi, H. Kawaguchi, S. Mizumoto, T. Kunihisa, M. Baba, Y. Kitayama, T. Takeuchi, R. M. Hoffman, R. Sasaki, *Anticancer Res.* **2020**, *40*, 3091.
- [78] H. Liu, W. Yuan, Q. Pang, C. Xue, X. Yan, *Talanta* **2022**, *239*, 123089.
- [79] W. Chen, Z. Li, P. Deng, Z. Li, Y. Xu, H. Li, W. Su, J. Qin, *Diagnostics* **2021**, *11*, 2151.
- [80] B.-K. Choi, X. Fan, H. Deng, N. Zhang, Z. An, *Cancer Med.* **2012**, *1*, 28.
- [81] J. Carlsson, H. Nordgren, J. Sjöström, K. Wester, K. Villman, N. O. Bengtsson, B. Ostenstad, H. Lundqvist, C. Blomqvist, *Br. J. Cancer* **2004**, *90*, 2344.
- [82] K. Subik, J.-F. Lee, L. Baxter, T. Strzepek, D. Costello, P. Crowley, L. Xing, M.-C. Hung, T. Bonfiglio, D. G. Hicks, P. Tang, *Breast Cancer (Auckl)* **2010**, *4*, 35.